INTERNATIONAL JOURNAL OF
ENERGY AND ENVIRONMENT

Volume 5, Issue 1, 2014 pp.85-96
Journal homepage: www.IJEE.IEEFoundation.org

Finite element modelling and simulation of free convection heat transfer in solar oven

Sobamowo M.G., Ogunmola B.Y., Ayerin A. M.

Department of Mechanical Engineering, University of Lagos, Akoka, Lagos, Nigeria.

Abstract
The use of solar energy for baking, heating or drying represents a sustainable way of solar energy applications with negligible negative effects. Solar oven is an alternative to conventional oven that rely heavily on coal and wood or Electric oven that uses the power from the National grid of which the end users have little or no control. Since the Solar oven uses no fuel and it costs nothing to run, it uses are widely promoted especially in situations where minimum fuel consumption or fire risks are considered highly important. As useful as the Solar Oven proved, it major setback in the area of applications has been its future sustainability. For the use of Solar Oven/Cookers to be sustained in the future, the design and development of solar oven must rely on sound analytical tools. Therefore, this work focused on the design and development of the solar oven. To test the performance of the Small Solar Oven a 5000cm^3 beaker of water was put into the Oven and the temperature of the water was found to reach 81^{0}C after about 3hrs under an average ambient temperature of 30^{0}C. On no load test, the oven reached a maximum temperature of 112^{o}C in 6hrs. In order to carry out the parametric studies and improve the performance of the Solar Oven, Mathematical models were developed and solved by using Characteristics-Based Split (CBS) Finite Element Method. The Model results were compared with the Experimental results and a good agreement was found between the two results.
Copyright © 2014 International Energy and Environment Foundation - All rights reserved.

Keywords: Solar energy; Free convection; Heat transfer; Solar oven; CBS finite element method.

1. Introduction

The world rapidly growing population and exploding energy demands coupled with the climatic profile, socio-economic development, energy supply infrastructures and the threats on health and environment accompanying the utilization of fossil fuels strongly suggest the use of renewable energy powered systems. In fact, the strategies for attaining balance between energy demands and effects in various countries has provoked vast majority in considering the alternative sources. Furthermore, the convergence of rapidly rising costs, dwindling and threatened supply of fossil fuel are stimulating renewed efforts to find viable energy alternatives. Some of the proposed alternatives such as large scale use of bio-fuels may not be achievable or sustainable-or, eventually practical. Some other interesting possibilities such as geothermal energy may be viable but are local and limited. Solar energy that is virtually an inexhaustible natural source produces little or no greenhouse gases. It is known as a clean and environmental friendly energy source. Aside from the indisputable advantages of solar energy mentioned above, the consideration of harnessing solar energy among all other alternative sources of energy sources to meet the needs especially in developing countries is based on well established visibility

studies. Firstly, most of the countries called developing, like Nigeria, are in or adjacent to the tropics and have good solar radiation available as shown in Figure 1. Secondly, energy is a critical need of these countries but they do not have widely distributed readily available supplies of conventional energy resources. Thirdly, most of the developing countries are characterized by arid climates, dispersed and inaccessible populations and a lack of investment capital and are thus faced with practically insuperable obstacles to the provision of energy by conventional means, for example, by electrification. In contrast to this, solar energy is readily available and is already distributed to the potential users. Fourthly, because of the diffuse nature of solar energy the developments all over the world, the energy source has been in smaller units which fit well into the pattern of rural economics.

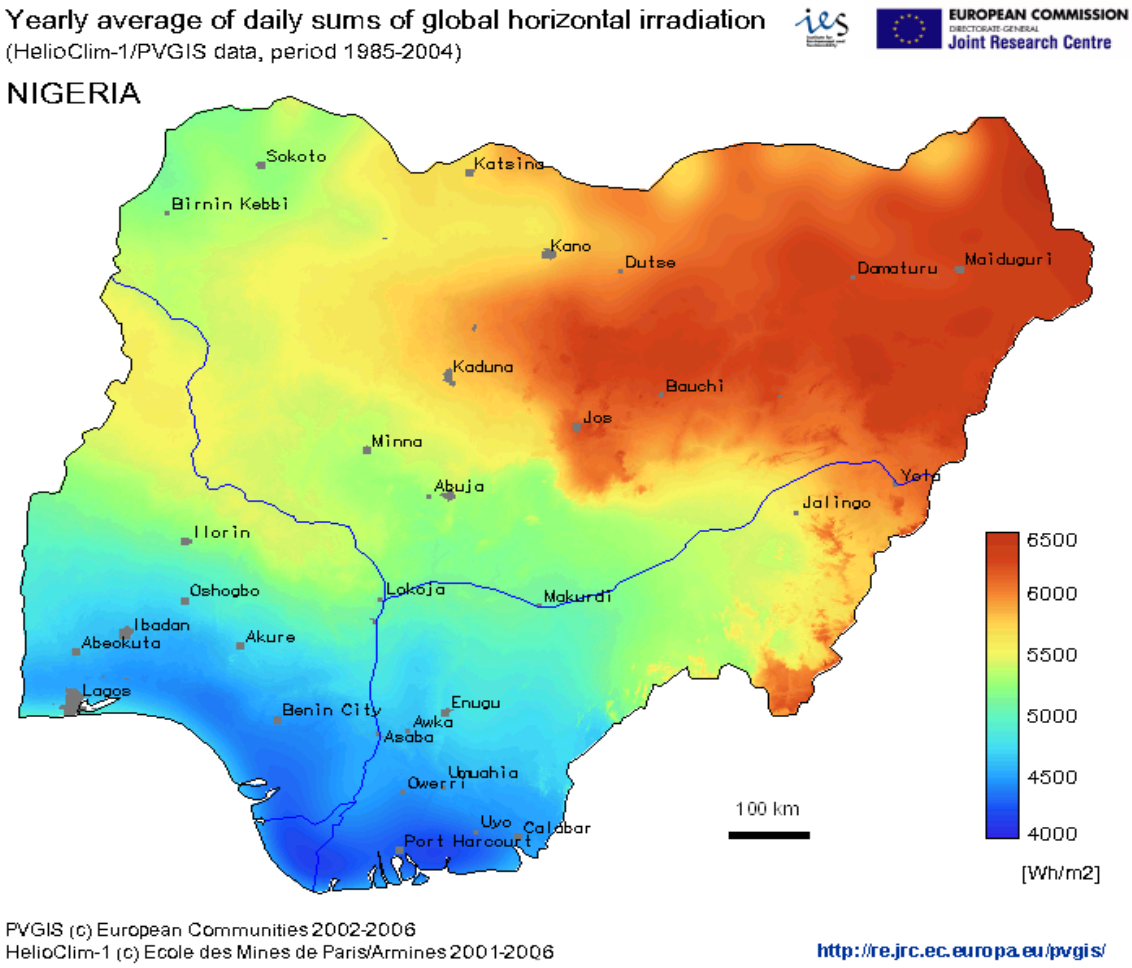

Figure 1. Solar insolation in different States in Nigeria

The abundant solar radiation in the tropical and subtropical regions proved solar energy as the most attractive a1ternative energy source for baking, cooking, drying and heating. A number of government, non-government and private organizations along with a few research institutions and other individual researchers have applied the knowledge of solar radiation on the earth surface for the fabrication, promotion and dissemination of different types of solar dryer (direct, indirect and mixed-mode types) in developing countries. In meeting the essential and basic need of human being, wood and fossil fuel as sources of energy for cooking food have played tremendous and invaluable roles. However, the direct combustion of wood and fossil fuel as the major sources of cooking has immensely contributed to global warming and acid rains. Aside from these adverse effects, the inhalation of these gases irritates the lungs and the eyes and can cause diseases such as pneumonia. In order to obviate or eliminate this problem, a lot of researchers [1-13] have developed different solar ovens/cookers over the years. The range of temperature achieved in most of these ovens/cookers (80^{o}C-100^{o}C) is most suitable for cooking by boiling. Talking about the advantages, this application of solar energy has been assisting in preventing deforestation, saving of fossil fuel and reduction in utility bills in most countries. Also, since the solar

 ©2014 International Energy & Environment Foundation. All rights reserved.

oven uses no fuel, it cost nothing to run and therefore, it use are widely promoted especially in situations where minimum fuel consumption or fire risks are considered highly important. However, as useful as the Solar Oven proved, it major setback in the area of applications has been its future sustainability. For the use of Solar Oven/Cookers to be sustained in the future, the design and development of solar oven must rely on sound analytical tools. Also, to understand the physical phenomena of solar oven and to optimize the performance of the forced convection solar dryer, theoretical investigation is essential. An adventure into the analytical methods in solving the resulting conservation equations for the theoretical investigations of the performance and optimisation of the Oven has proven abortive and over the years, recourse has been made to numerical methods such as Finite difference or Finite volume methods in analysing such class of problems involving conduction, convection and sometimes diffusion. The finite element method has been somehow stated to be limited to Computational Solid Mechanic or at its best in Thermo-Fluid problems, conductive heat transfer. Actually, for most conduction equations in heat transfer problems, the finite element method especially Galerkin Method is straight forward. However, if similar Garlerkin type approximation is applied in the solution of convection equations, the results will be marked with spurious oscillations in space if certain parameters exceed a critical value, element peclet number. This method is not unique to finite elements as all other spatial discretization techniques techniques have difficulties. Direct application of the Characteristic Galerkin scheme to solve the momentum equation is difficult. Therefore, in this work, a Characteristic Based Split (CBS) scheme which satisfies the well-known Babuska-Brezzi condition [14, 15] as proposed by Lewis *et al.* [16] is used to analysis and simulates the heat transfer in a photovoltaic-powered forced convection solar dryer. In order to optimize the performance of the solar dryer, the developed finite element models were used to investigate the effects of the blower speeds and the solar dryer chamber aspect ratios on the temperature distribution, velocity distribution and the pressure drop in the drying chamber.

2. The working principle of solar oven and experimental set up

When solar energy is radiated on the solar collector of the solar oven (Figure 2), some of energy is reflected, some is absorbed or some of it passes right through. But only the absorbed energy is converted heat energy in the enclosure of the solar oven. When food is placed in this solar oven enclosure, moisture at the surface is evaporated and removed by the hot air and the low humidity of air in the oven. This establishes moisture vapour pressure gradient, which causes movement of moisture from the interior of the food to the surface. Depending on the nature of the food and the rate of heating when the extent of moisture loss exceeds the rate of movement from the interior, the zone of evaporation moves inside the food, the surface dried out, the temperature rise to the temperature of the hot air (119°-240°C) and a crust is formed but the internal temperature of the food does not exceed 100°C cause baking takes place at atmospheric pressure and moisture escape freely from the food.

Figure 2. Physical model of the solar oven

 ©2014 International Energy & Environment Foundation. All rights reserved.

Since the food does not reach too high temperature in the oven, it can safely be left in the cooker all day without burning. Depending on the latitude and weather, food can be cooked or baked either early or later in the day. The cooker can also be used to warm food, drinks and pasteurize water or milk.
The two test carried above was conducted on solar oven. The results obtained are shown in Figures 3 and 4. The test at load which involved placing of 500cm3 beaker of water.

3. Model development for the solar oven

The numerical investigations of the solar oven involve setting up mathematical models. In order to achieve this, a set of conservation equations were set up for the numerical analysis

3.1 Conservation equations for the analysis of solar oven

The following set of conservation equations were used for the finite element analysis.

Continuity equation

$$\frac{\partial u}{\partial x} + \frac{\partial v}{\partial y} = 0 \quad (1)$$

x-momentum equation

$$\frac{\partial u}{\partial t} + u\frac{\partial u}{\partial x} + v\frac{\partial u}{\partial y} = -\frac{1}{\rho}\frac{\partial p}{\partial x} + v\left[\frac{\partial^2 u}{\partial x^2} + \frac{\partial^2 u}{\partial y}\right] \quad (2)$$

y-momentum equation

$$\frac{\partial v}{\partial t} + u\frac{\partial v}{\partial x} + v\frac{\partial v}{\partial y} = -\frac{1}{\rho}\frac{\partial p}{\partial y} + v\left[\frac{\partial^2 v}{\partial x^2} + \frac{\partial^2 v}{\partial y^2}\right] + \beta g(T - T_o) \quad (3)$$

Energy equation

$$\frac{\partial T}{\partial t} + u\frac{\partial T}{\partial x} + v\frac{\partial T}{\partial y} = \alpha\left[\frac{\partial^2 T}{\partial x^2} + \frac{\partial^2 T}{\partial y^2}\right] \quad (4)$$

The initial conditions used in this model are: $t = 0,\quad u = 0,\ v = 0,\ T = T_\infty,\ p = p_\infty\ \ for\ 0 < x < L, 0 < y < L$

The boundary conditions used in this model are: $t > 0,\quad y = 0,\quad u = v = 0,\quad \frac{\partial T}{\partial y} = 0,\quad \frac{\partial p}{\partial y} = 0\quad for\ 0 < x < L$

$$\begin{aligned} &t > 0, \quad y = L, \quad u = v = 0, \quad T = T_w, \quad p = p_m \quad for\ 0 < x < L \\ &t > 0, \quad x = 0 \quad u = v = 0, \quad \frac{\partial T}{\partial x} = 0, \quad \frac{\partial p}{\partial x} = 0 \quad for\ 0 < y < L \\ &t > 0, \quad x = L \quad u = v = 0, \quad \frac{\partial T}{\partial x} = 0, \quad \frac{\partial p}{\partial x} = 0 \quad for\ 0 < y < L \end{aligned} \quad (5a)$$

To obtain the non-dimensional form of the equation, the following non-dimentional scales are used.

$$X = \frac{x}{L},\ Y = \frac{y}{L},\ \tau = \frac{tu_\infty}{L},\ U = \frac{u}{U_\infty},\ V = \frac{v}{U_\infty},\ P = \frac{p}{\rho U^2{}_\infty},\ \theta = \frac{T - T_\infty}{T_w - T_\infty} \quad (5b)$$

where L is the characteristics dimention, T_w is the wall temperature (reference temperature) and U_∞ is the free stream velocity.
Substituting the above scales into equations (1-4), we have:

Continuity equation

$$\frac{\partial U}{\partial X} + \frac{\partial V}{\partial Y} = 0 \quad (6)$$

 ©2014 International Energy & Environment Foundation. All rights reserved.

X-momentum equation

$$\frac{\partial V}{\partial \tau} + U\frac{\partial U}{\partial X} + V\frac{\partial U}{\partial Y} = -\frac{\partial P}{\partial Y} + \frac{1}{Re}\left(\frac{\partial^2 U}{\partial X^2} + \frac{\partial^2 U}{\partial X^2}\right) \quad (7)$$

Y-momentum equation

$$\frac{\partial V}{\partial \tau} + U\frac{\partial V}{\partial X} + V\frac{\partial V}{\partial Y} = -\frac{\partial P}{\partial Y} + \frac{1}{Re}\left(\frac{\partial^2 V}{\partial X^2} + \frac{\partial^2 V}{\partial X^2}\right) + \frac{Gr}{Re^2}\theta \quad (8)$$

Energy equation

$$\frac{\partial \theta}{\partial \tau} + U\frac{\partial \theta}{\partial X} + V\frac{\partial \theta}{\partial Y} = \frac{1}{RePr}\left(\frac{\partial^2 \theta}{\partial X^2} + \frac{\partial^2 \theta}{\partial X^2}\right) \quad (9)$$

or

$$\frac{\partial \theta}{\partial \tau} + U\frac{\partial \theta}{\partial X} + V\frac{\partial \theta}{\partial Y} = \frac{1}{Pe}\left(\frac{\partial^2 \theta}{\partial X^2} + \frac{\partial^2 \theta}{\partial X^2}\right) \quad (10)$$

The initial and Boundary conditions in dimensionless form are:

$$\begin{aligned}
&\tau > 0, \quad Y = 0, \quad U = V = 0, \quad \frac{\partial \theta}{\partial Y} = 0, \quad \frac{\partial P}{\partial Y} = 0 \quad for\ 0 < X < 1\\
&\tau > 0, \quad Y = 1, \quad U = V = 0, \quad T = 1, \quad P = p_m/\rho U^2 \quad for\ 0 < X < 1\\
&\tau > 0, \quad X = 0 \quad U = V = 0, \quad \frac{\partial \theta}{\partial X} = 0, \quad \frac{\partial P}{\partial X} = 0 \quad for\ 0 < y < 1\\
&\tau > 0,\ X = 1 \quad U = V = 0,\ \frac{\partial \theta}{\partial X} = 0,\ \frac{\partial P}{\partial X} = 0 \quad for\ 0 < y < 1
\end{aligned} \quad (11)$$

3.2 Characteristics-based split (CBS) finite element analysis of the conservation equations
For the continuity equation

$$\frac{U^n_{i+1,j} - U^n_{i,j}}{\Delta X} + \frac{V^n_{i+1,j} - V^n_{i,j}}{\Delta Y} = 0 \quad \text{or} \quad \frac{\partial U^n_{ij}}{\partial X} + \frac{\partial V^n_{ij}}{\partial X} \quad (12)$$

For the x-momentum equation, the semi-discrete form is:

$$\frac{U^{n+1}_{ij} - U^n_{ij}}{\Delta \tau} = U^n_{ij}\frac{\partial U^n_{ij}}{\partial X} - V^n_{ij}\frac{\partial U^n_{ij}}{\partial Y} + \frac{1}{Re}\left(\frac{\partial^2 U_{ij}}{\partial X^2} + \frac{\partial^2 V_{ij}}{\partial Y^2}\right)^n - \frac{\partial P_{ij}}{\partial X} + U_{ij}\frac{\Delta \tau}{2}\frac{\partial}{\partial X}\left[U^n_{ij}\frac{\partial U^n_{ij}}{\partial X} + V^n_{ij}\frac{\partial U^n_{ij}}{\partial Y} + \frac{\partial P^n_{ij}}{\partial X}\right] + V_{ij}\frac{\Delta \tau}{2}\frac{\partial}{\partial Y}\left[U^n_{ij}\frac{\partial U^n_{ij}}{\partial X} + V^n_{ij}\frac{\partial U^n_{ij}}{\partial Y} + \frac{\partial P^n_{ij}}{\partial X}\right] \quad (13a)$$

For y-momentum equation, the semi-discrete form is:

$$\frac{V^{n+1}_{ij} - V^n_{ij}}{\Delta \tau} = U^n_{ij}\frac{\partial V^n_{ij}}{\partial X} - V^n_{ij}\frac{\partial V^n_{ij}}{\partial Y} + \frac{1}{Re}\left(\frac{\partial^2 V_{ij}}{\partial X^2} + \frac{\partial^2 V_{ij}}{\partial Y^2}\right)^n - \frac{\partial P_{ij}}{\partial X} + U_{ij}{}^n\frac{\Delta \tau}{2}\frac{\partial}{\partial X}\left[U^n_{ij}\frac{\partial U^n_{ij}}{\partial X} + V^n_{ij}\frac{\partial U^n_{ij}}{\partial Y} + \frac{\partial P^n_{ij}}{\partial X}\right] + V_{ij}{}^n\frac{\Delta \tau}{2}\frac{\partial}{\partial Y}\left[U^n_{ij}\frac{\partial V^n_{ij}}{\partial X} + V^n_{ij}\frac{\partial V^n_{ij}}{\partial Y} + \frac{\partial P^n_{ij}}{\partial X}\right] + \frac{Gr}{Re^2}\theta^n_{ij} \quad (13b)$$

On removing the pressure from equations 13a and 13b, we arrived equations 14-15

$$\frac{U_{ij} - U^n_{ij}}{\Delta \tau} = U^n_{ij}\frac{\partial U^n_{ij}}{\partial X} - V^n_{ij}\frac{\partial U^n_{ij}}{\partial Y} + \frac{1}{Re}\left(\frac{\partial^2 U_{ij}}{\partial X^2} + \frac{\partial^2 U_{ij}}{\partial Y^2}\right)^n + U_{ij}{}^n\frac{\Delta \tau}{2}\frac{\partial}{\partial X}\left(U^n_{ij}\frac{\partial U^n_{ij}}{\partial X} + V^n_{ij}\frac{\partial U^n_{ij}}{\partial Y}\right) + V^n_{ij}\frac{\Delta \tau}{2}\frac{\partial}{\partial Y}\left(U^n_{ij}\frac{\partial U^n_{ij}}{\partial X} + V^n_{ij}\frac{\partial U^n_{ij}}{\partial Y}\right) \quad (14)$$

 ©2014 International Energy & Environment Foundation. All rights reserved.

$$\frac{V_{ij}-V_{ij}^{n}}{\Delta\tau}=U_{ij}^{n}\frac{\partial V_{ij}^{n}}{\partial X}-V_{ij}^{n}\frac{\partial V_{ij}^{n}}{\partial Y}+\frac{1}{Re}\left(\frac{\partial^{2}V_{ij}}{\partial X^{2}}+\frac{\partial^{2}V_{ij}}{\partial Y^{2}}\right)^{n}+U_{ij}^{n}\frac{\Delta\tau}{2}\frac{\partial}{\partial X}\left(U_{ij}^{n}\frac{\partial U_{ij}^{n}}{\partial X}+V_{ij}^{n}\frac{\partial U_{ij}^{n}}{\partial Y}\right)+V_{ij}^{n}\frac{\Delta\tau}{2}\frac{\partial}{\partial Y}\left(U_{ij}^{n}\frac{\partial V_{ij}^{n}}{\partial X}+Vijn\partial Vijn\partial Y+GrRe2\theta ijn\right) \quad 15$$

By subtracting equations 14 and 15 from equations 13a and 13b respectively, we obtained the real velocity field equations(velocity or momentum correction equations) as:

$$\frac{U_{ij}^{n+1}-\bar{U}_{ij}}{\Delta\tau}=-\frac{\partial P^{n}}{\partial X}+U\frac{\Delta\tau}{2}\frac{\partial}{\partial X}\left(\frac{\partial P}{\partial X}\right)^{n}+V\frac{\Delta\tau}{2}\frac{\partial}{\partial X}\left(\frac{\partial P}{\partial X}\right)^{n} \quad 16$$

$$\frac{V_{ij}^{n+1}-\bar{V}_{ij}}{\Delta\tau}=-\frac{\partial P^{n}}{\partial Y}+U\frac{\Delta\tau}{2}\frac{\partial}{\partial X}\left(\frac{\partial P}{\partial X}\right)^{n}+V\frac{\Delta\tau}{2}\frac{\partial}{\partial Y}\left(\frac{\partial P}{\partial Y}\right)^{n} \quad 17$$

Differentiating equation 17 with respect to X and also with respect to Y and adding the resulting equations together neglecting third-order terms gives.

$$\frac{\partial U_{ij}^{n+1}}{\partial \mathrm{X}}+\frac{\partial V_{ij}^{n+1}}{\partial \mathrm{Y}}-\frac{\partial \bar{U}_{ij}}{\partial X}-\frac{\partial \bar{V}_{ij}}{\partial Y}=-\Delta\tau\left(\frac{\partial^{2}P_{ij}}{\partial X^{2}}+\frac{\partial^{2}P_{ij}}{\partial Y^{2}}\right)^{n} \quad 18$$

Which gives the pressure calculation

$$\left(\frac{\partial^{2}P_{ij}}{\partial X^{2}}+\frac{\partial^{2}P_{ij}}{\partial Y^{2}}\right)^{n}=\frac{1}{\Delta\tau}\left(\frac{\partial \bar{U}_{ij}{}^{n}}{\partial X}+\frac{\partial \bar{V}_{ij}{}^{n}}{\partial Y}\right) \quad 19$$

Since (continuity equation);

$$\frac{\partial U_{ij}^{n+1}}{\partial \mathrm{X}}+\frac{\partial V_{ij}^{n+1}}{\partial \mathrm{Y}}=0 \quad 20$$

Temperature calculation

Applying the characteristic Galerkin procedure to the temperature equation (11), it gives:

$$\frac{\theta_{ij}^{n+1}-\theta_{ij}^{n}}{\Delta t}=U_{ij}^{n}\frac{\partial\theta^{n}}{\partial X}-V_{ij}^{n}\frac{\partial\theta_{ij}^{n}}{\partial Y}+\frac{1}{Re\,P_{r}}\left(\frac{\partial^{2}\theta_{ij}}{\partial X^{2}}+\frac{\partial^{2}\theta_{ij}}{\partial Y^{2}}\right)^{n}+U\frac{\Delta\tau}{2}\frac{\partial}{\partial X}\left(U\frac{\partial\theta}{\partial X}+V\frac{\partial\theta}{\partial Y}\right)+V\frac{\Delta\tau}{2}\frac{\partial}{\partial Y}\left(U\frac{\partial\theta}{\partial X}+V\partial\theta\partial Yn\right) \quad 21$$

In summary, we have the intermediate X-momentum equation is:

$$\frac{\bar{U}_{ij}-\bar{U}_{ij}^{n}}{\Delta t}=U\frac{\partial U_{ij}^{n}}{\partial X}-V\frac{\partial U_{ij}^{n}}{\partial X}+\frac{1}{Re}\left(\frac{\partial^{2}U_{ij}}{\partial X^{2}}+\frac{\partial^{2}U_{ij}}{\partial Y^{2}}\right)^{n}+U_{ij}^{n}\frac{\Delta\tau}{2}\frac{\partial}{\partial X}\left(U_{ij}^{n}\frac{\partial V_{ij}}{\partial X}+V\frac{\partial V_{ij}}{\partial Y}\right)^{n}+V_{ij}^{n}\frac{\Delta\tau}{2}\frac{\partial}{\partial Y}\left(U_{ij}^{n}\frac{\partial U_{ij}}{\partial X}+V\partial Uij\partial Y\right) \quad 22$$

And the intermediate Y-momentum equation is:

$$\frac{\bar{V}_{ij}-\bar{V}_{ij}^{n}}{\Delta t}=U_{ij}\frac{\partial V_{ij}^{n}}{\partial X}-V\frac{\partial V_{ij}^{n}}{\partial Y}+\frac{1}{Re}\left(\frac{\partial^{2}V_{ij}}{\partial X^{2}}+\frac{\partial^{2}V_{ij}}{\partial Y^{2}}\right)^{n}+U_{ij}^{n}\frac{\Delta\tau}{2}\frac{\partial}{\partial X}\left(U_{ij}^{n}\frac{\partial V_{ij}}{\partial X}+V\frac{\partial V_{ij}}{\partial Y}\right)^{n}+V_{ij}^{n}\frac{\Delta\tau}{2}\frac{\partial}{\partial Y}\left(U\frac{\partial U_{ij}}{\partial X}+V\partial Uij\partial Y\right) \quad 23$$

Pressure calculation

$$\left(\frac{\partial^{2}P_{ij}}{\partial X^{2}}+\frac{\partial^{2}P_{ij}}{\partial Y^{2}}\right)^{n}=\frac{1}{\Delta\tau}\left(\frac{\partial \bar{U}_{1}}{\partial X}+\frac{\partial \bar{V}}{\partial Y}\right) \quad 24$$

 ©2014 International Energy & Environment Foundation. All rights reserved.

Temperature equation

$$\frac{\theta_{ij}^{n+1}-\theta_{ij}^{n}}{\Delta t} = U_{ij}^{n}\frac{\partial \theta^{n}}{\partial X} - V_{ij}^{n}\frac{\partial \theta_{ij}^{n}}{\partial Y} + \frac{1}{Re\,P_r}\left(\frac{\partial^2\theta_{ij}}{\partial X^2}+\frac{\partial^2\theta_{ij}}{\partial Y^2}\right)^{n} + U\frac{\Delta\tau}{2}\frac{\partial}{\partial X}\left(U\frac{\partial\theta}{\partial X}+V\frac{\partial\theta}{\partial Y}\right) + V\frac{\Delta\tau}{2}\frac{\partial}{\partial Y}\left(U\frac{\partial\theta}{\partial X}+ V\partial\theta\partial Yn\right) \quad 25$$

Spatial discretization

Applying the standard Galerkin approximation for solving equations 20-25, assuming linear interpolation functions for all variables, the spatial variation for a linear triangular element may be written as:

$$U = N_i U_i + N_j U_j + N_k U_k = [N][U] \quad 26$$

$$V = N_i V_i + N_j V_j + N_k V_k = [N][V] \quad 27$$

$$P = N_i P_i + N_j P_j + N_k P_k = [N][P] \quad 28$$

$$\theta = N_i \theta_i + N_j \theta_j + N_k \theta_k = [N][\theta] \quad 29$$

After performing spatial discretization, the Element Mass Matrix from the Characteristics-Based Split scheme is:

$$[M_e] = \frac{A}{12}\begin{bmatrix}2 & 1 & 1\\ 1 & 2 & 1\\ 1 & 1 & 2\end{bmatrix} \quad 30$$

And the Element Convection Matrix

$$[C_e] = \frac{1}{24}\begin{bmatrix}(wsw+u_i)b_i & (wsw+u_i)b_j & (wsw+u_i)b_k\\ (wsw+u_j)b_i & (wsw+u_j)b_j & (wsw+u_j)b_k\\ (wsw+u_k)b_i & (wsw+u_k)b_j & (wsw+u_k)b_k\end{bmatrix} + \frac{1}{24}\begin{bmatrix}(wrw+u_i)c_i & (wrw+u_i)c_j & (wrw+u_i)c_k\\ (wrw+u_j)c_i & (wrw+u_j)c_j & (wrw+u_j)c_k\\ (wrw+u_k)c_i & (wrw+u_k)c_j & (wrw+u_k)c_k\end{bmatrix} \quad 31$$

where

$wsw = u_i + u_j + u_k$, $wrw = v_i + v_j + v_k$

$$[K_e] = \frac{Re}{4A}\begin{bmatrix}b_i^2 & b_i b_j & b_i b_k\\ b_j b_i & b_j^2 & b_j b_k\\ b_k b_i & b_k b_j & b_k^2\end{bmatrix} + \frac{Re}{4A}\begin{bmatrix}c_i^2 & c_i c_j & c_i c_k\\ c_j c_i & c_j^2 & c_j c_k\\ c_k c_i & c_k c_j & c_k^2\end{bmatrix} \quad 32$$

For the momentum diffussion, we have;

$$[K_{te}] = \frac{P_r}{4A}\begin{bmatrix}b_i^2 & b_i b_j & b_i b_k\\ b_j b_i & b_j^2 & b_j b_k\\ b_k b_i & b_k b_j & b_k^2\end{bmatrix} + \frac{P_r}{4A}\begin{bmatrix}c_i^2 & c_i c_j & c_i c_k\\ c_j c_i & c_j^2 & c_j c_k\\ c_k c_i & c_k c_j & c_k^2\end{bmatrix} \quad 33$$

And for the Heat diffusion and Stabilization Matrix

 ©2014 International Energy & Environment Foundation. All rights reserved.

$$[K_{se}] = \frac{U_{av}}{12}\begin{bmatrix} b_i^2 & b_i b_j & b_i b_k \\ b_j b_i & b_j^2 & b_j b_k \\ b_k b_i & b_k b_j & b_k^2 \end{bmatrix} + \frac{U_{av}}{12}\begin{bmatrix} b_i c_i & b_i c_j & b_i c_k \\ b_j c_i & b_j c_j & b_j c_k \\ b_k c_i & b_k c_j & b_k c_k \end{bmatrix} + \frac{V_{av}}{12A}\begin{bmatrix} c_i b_i & c_i b_j & c_i b_k \\ c_j b_i & c_j b_j & c_j b_k \\ c_k b_i & c_k b_j & c_k b_k \end{bmatrix} + \frac{V_{av}}{12A}\begin{bmatrix} c_i^2 & c_i c_j & c_i c_k \\ c_j c_i & c_j^2 & c_j c_k \\ c_k c_i & c_k c_j & c_k^2 \end{bmatrix} \quad (34)$$

where U_{av} and V_{av} are the average values of U and V over the element. The discretization of the CBS steps requires three more matrices and four forcing vectors to complete the process. The matrix from the discretized second-order terms for pressure calculations is:

$$K = \frac{1}{4A}\begin{bmatrix} b_i^2 & b_i b_j & b_i b_k \\ b_j b_i & b_j^2 & b_j b_k \\ b_k b_i & b_k b_j & b_k^2 \end{bmatrix} + \frac{1}{4A}\begin{bmatrix} c_i^2 & c_i c_j & c_i c_k \\ c_j c_i & c_j^2 & c_j c_k \\ c_k c_i & c_k c_j & c_k^2 \end{bmatrix} \quad (35)$$

The first gradient matrix in the X-direction is:

$$[G_u] = \frac{1}{6}\begin{bmatrix} b_i & b_j & b_k \\ b_i & b_j & b_k \\ b_i & b_j & b_k \end{bmatrix} \quad (36)$$

And the second-gradient matrix in the Y-direction is

$$[G_v] = \frac{1}{6}\begin{bmatrix} c_i & c_j & c_k \\ c_i & c_j & c_k \\ c_i & c_j & c_k \end{bmatrix} \quad (37)$$

The forcing vectors of the X-component of the momentum equation is:

$$[f_1] = \frac{\Gamma}{4A} Re \begin{bmatrix} b_i u_i & b_j u_j & b_k u_k \\ b_i u_i & b_j u_j & b_k u_k \\ 0 & 0 & 0 \end{bmatrix}^n n_u + \frac{\Gamma}{4A} Re \begin{bmatrix} c_i u_i & c_j u_j & c_k u_k \\ c_i u_i & c_j u_j & cb_k u_k \\ 0 & 0 & 0 \end{bmatrix}^n n_v \quad (38)$$

where $i\ j$ is the boundary edge of an element.
The forcing vector of the Y- component momentum equation is:

$$[f_2] = \frac{\Gamma}{4A} Re \begin{bmatrix} b_i v_i & b_j v_j & b_k v_k \\ b_i v_i & b_j v_j & b_k v_k \\ 0 & 0 & 0 \end{bmatrix}^n n_u + \frac{\Gamma}{4A} Re \begin{bmatrix} c_i v_i & c_j v_j & c_k v_k \\ c_i v_i & c_j v_j & c_k v_k \\ 0 & 0 & 0 \end{bmatrix}^n n_v \quad (39)$$

The forcing vector from the discretion of the second-order pressure terms in pressure calculations is:

$$[f_3] = \frac{\Gamma}{4A} \begin{bmatrix} b_i P_i & b_j P_j & b_k P_k \\ b_i P_i & b_j P_j & b_k P_k \\ 0 & 0 & 0 \end{bmatrix}^n n_u + \frac{\Gamma}{4A} \begin{bmatrix} c_i P_i & c_j P_j & c_k P_k \\ c_i P_i & c_j P_j & c_k P_k \\ 0 & 0 & 0 \end{bmatrix}^n n_v \quad (40)$$

Finally, the forcing term due to the discretization of the second-order terms in the equation is:

$$[f_4] = \frac{\Gamma}{4A} Pr \begin{bmatrix} b_i \theta_i & b_j \theta_j & b_k \theta_k \\ b_i \theta_i & b_j \theta_j & b_k \theta_k \\ 0 & 0 & 0 \end{bmatrix}^n n_u + \frac{\Gamma}{4A} P_r \begin{bmatrix} c_i \theta_i & c_j \theta_j & c_k \theta_k \\ c_i \theta_i & c_j \theta_j & c_k \theta_k \\ 0 & 0 & 0 \end{bmatrix}^n n_v \quad (41)$$

 ©2014 International Energy & Environment Foundation. All rights reserved.

The four steps of the characteristic based split scheme may now be written in matrix form.

Step 1: Intermediate Velocity Calculation X-Component

$$\left[\boldsymbol{M}\frac{\Delta[\widetilde{U}]}{\Delta \mathbf{t}}\right] = -[\boldsymbol{C}][\boldsymbol{U}]^{\boldsymbol{n}} - [\boldsymbol{K_m}][\boldsymbol{U}]^{\boldsymbol{n}} - [\boldsymbol{K_b}][\boldsymbol{U}]^{\boldsymbol{n}} + [\boldsymbol{f_1}] \quad 42$$

Intermediate Velocity Calculation Y-Component

$$\left[\boldsymbol{M}\frac{\Delta[\widetilde{U}]}{\Delta \mathbf{t}}\right] = -[\boldsymbol{C}][\boldsymbol{V}]^{\boldsymbol{n}} - [\boldsymbol{K_m}][\boldsymbol{V}]^{\boldsymbol{n}} - [\boldsymbol{K_s}][\boldsymbol{V}]^{\boldsymbol{n}} + [\boldsymbol{f_2}] \quad 43$$

Step 2: Pressure Calculation

$$[\boldsymbol{K}][\boldsymbol{P}]^{\boldsymbol{n}} = -\frac{\mathbf{1}}{\Delta \mathbf{t}}[\boldsymbol{G_u}]\left[\widetilde{\boldsymbol{U}}\right] + [\boldsymbol{G_u}]\left[\widetilde{\boldsymbol{V}}\right] + [\boldsymbol{f_3}] \quad 44$$

Step 3: Velocity Correction

$$[\boldsymbol{M}][\boldsymbol{U}]^{\boldsymbol{n+1}} = [\boldsymbol{M}]\left[\widetilde{\boldsymbol{U}}\right] - \boldsymbol{\Delta\tau}[\boldsymbol{G_v}][\boldsymbol{P}]^{\boldsymbol{n}} \quad 45a$$

$$[\boldsymbol{M}][\boldsymbol{V}]^{[\boldsymbol{n+1}} = [\boldsymbol{M}]\left[\widetilde{\boldsymbol{V}}\right] - \boldsymbol{\Delta\tau}[\boldsymbol{G_v}][\boldsymbol{P}]^{\boldsymbol{n}} \quad 45b$$

Step 4: Temperature Computation

$$\left[\boldsymbol{M}\frac{\Delta[\boldsymbol{\theta}]}{\Delta \mathbf{t}}\right] = -[\boldsymbol{C}][\boldsymbol{\theta}]^{\boldsymbol{n}} - \left[\boldsymbol{K_f}\right][\boldsymbol{\theta}]^{\boldsymbol{n}} - [\boldsymbol{K_s}][\boldsymbol{\theta}]^{\boldsymbol{n}} + [\boldsymbol{f_4}] \quad 46$$

4. Results and discussion

Following the unstructured and adaptive mesh generation techniques, a two-dimensional element of triangular shape is used. Figure 3 shows the finite element discretization for two-dimensional solution procedures as employed in this work. Figure 4 shows the Finite element solution for the temperature distribution in the solar oven after 30min. From the figure, the highest temperature 50^{o}C was found to be at the top of the oven. This is because, it is the part of the solar oven that directly receives solar radiative heat from the sun as the solar energy from the sun strikes the solar collector on the top of the oven. The lowest temperature in the solar panel after about 30mins was recorded to be 35^{o}C and this was found to be at the bottom of the oven. This is because, as the heat travel from the top of the oven to the bottom, there is a temperature drop due to the heat convected by the actual movement of air molecules in the solar oven chamber. Also, during this period, the average temperature found in the oven is approximately 42.5^{o}C.

Figure 5 displays the pressure distribution in the oven after 30 min. As the solar oven is exposed to solar radiation for a period of 2hrs 30mins, the solar oven temperature increases as more radiative heat is received from the sun by the solar collector. The temperature and pressure distributions at this time are shown in Figures 6 and 7.

The finite element simulated results of the temperature and pressure distributions after a period of 4hrs 30mins of receiving direct radiation from the sun are shown in Figures 8 and 9 while Figures 10, 11 and 12 depict temperature and pressure and velocity distributions after about 6hrs. The simulated results shown above are the results of what happened in the solar oven chamber during a period of 6hours of maximum insolation. From these results, the maximum temperature in oven predicted by the finite element method is 117^{o}C and the pressure in the oven increases as the temperature increases.

Figure 13 shows the experimental results of the average temperature of the solar oven and the ambient. The test was set out around 8am of 8th October, 2005. From the results, it was discovered that the time taken for the oven to attain a maximum temperature of 112°C was 6hours without the average insolation on no load. Figure 14 shows the comparison of the predicted results with the experimental results. As it could be seen from the figure, a good agreement was achieved between the predicted results of the numerical analysis and the experimental results.

 ©2014 International Energy & Environment Foundation. All rights reserved.

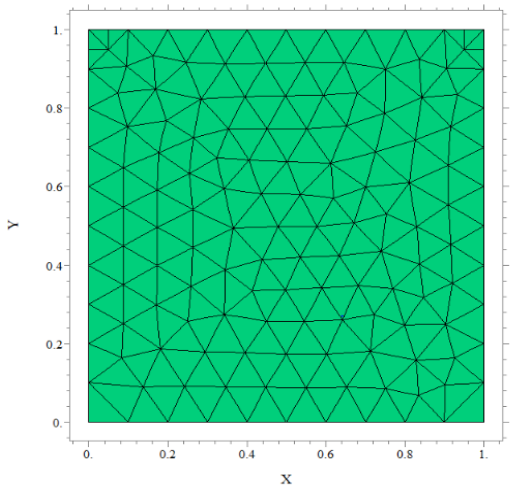

Figure 3. The finite element discretization of the solar oven enclosure

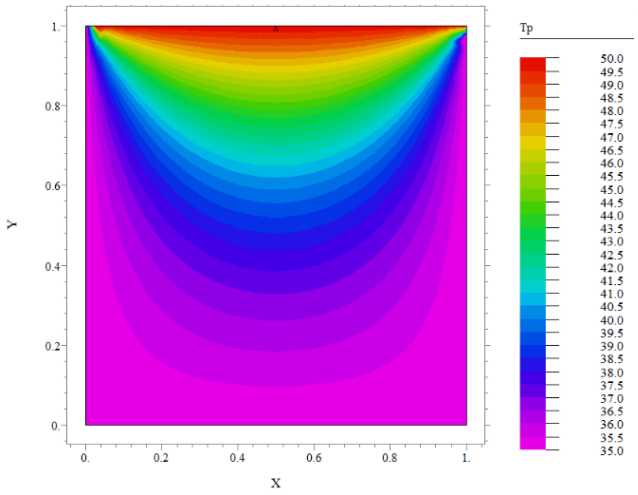

Figure 4. Temperature distribution in the oven after 30 mins

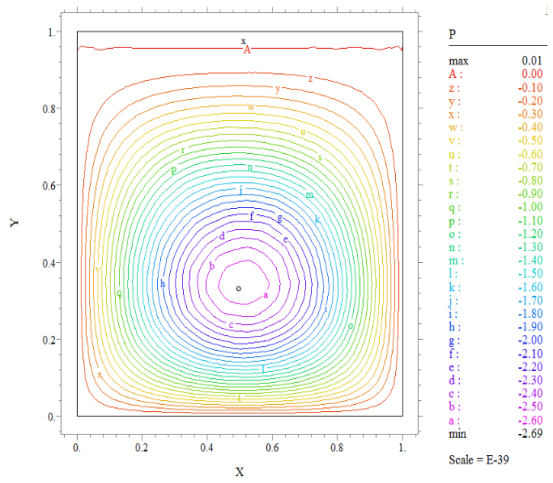

Figure 5. Pressure distribution in the oven after 30 mins

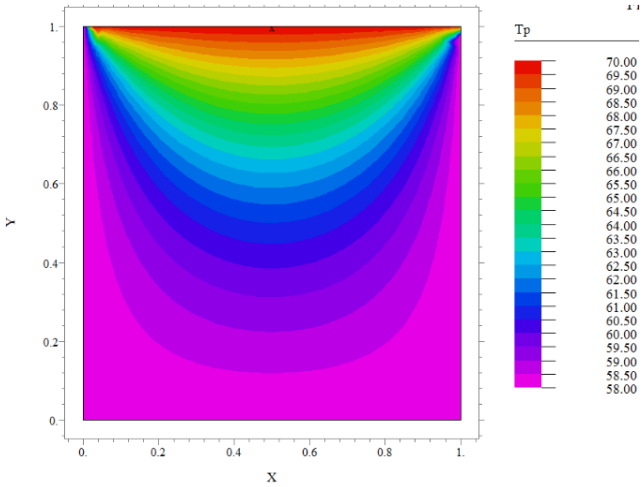

Figure 6. Temperature distribution in the oven after 2 hrs 30 mins

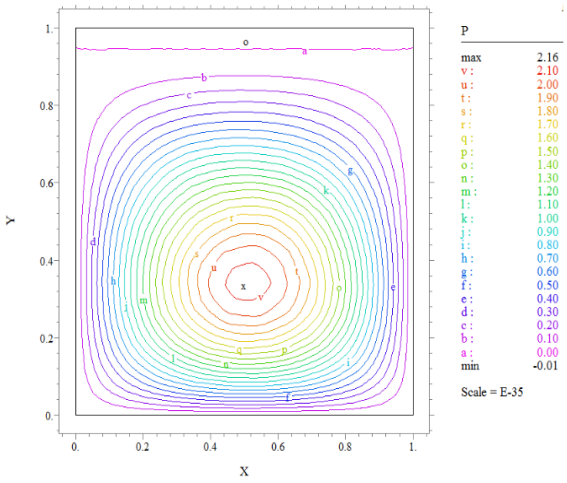

Figure 7. Pressure distribution in the oven after 2 hrs 30 mins

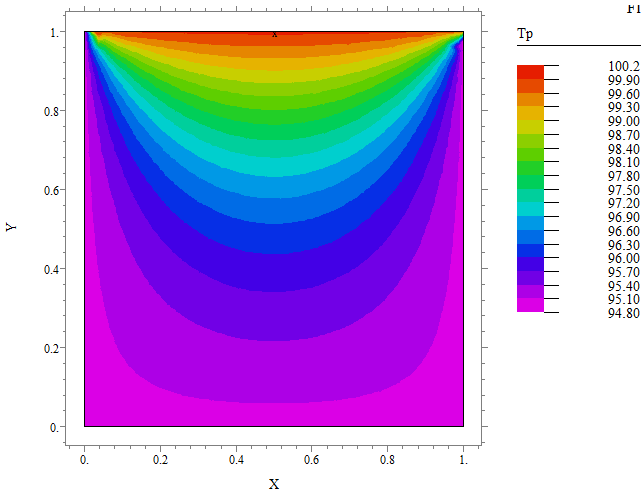

Figure 8. Temperature distribution in the oven after 4 hrs 30 mins

 ©2014 International Energy & Environment Foundation. All rights reserved.

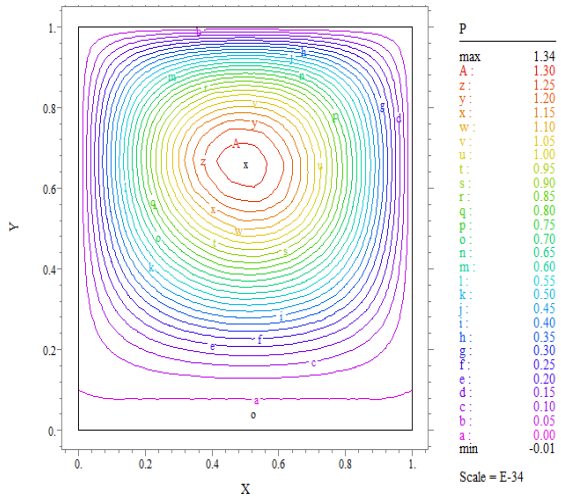

Figure 9. Pressure distribution in the oven after 4 hrs 30 mins

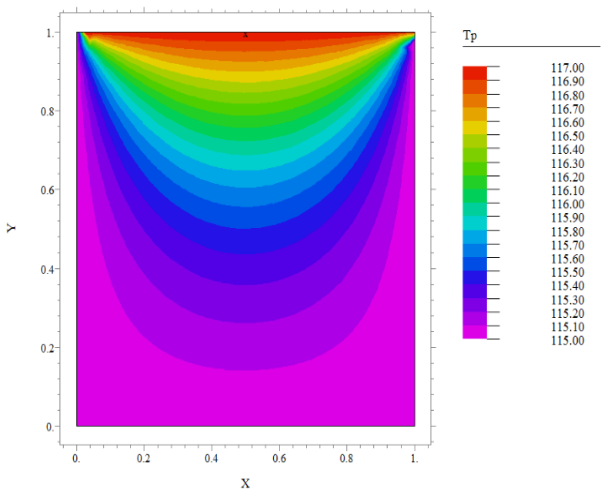

Figure 10. Temperature distribution in the oven after 6 hrs

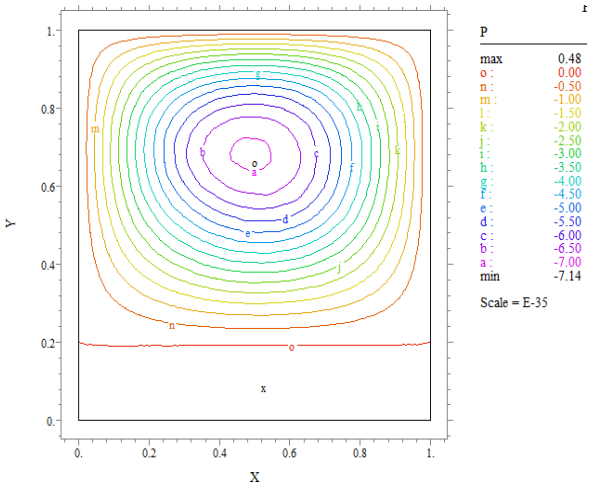

Figure 11. Pressure distribution in the oven after 6 hrs

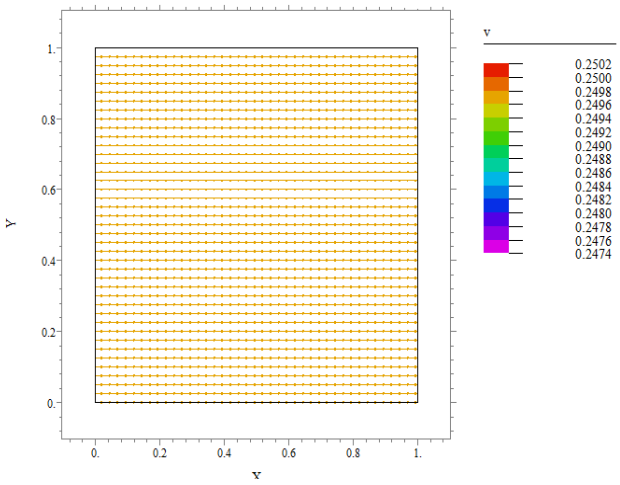

Figure 12. Velocity distribution in the oven after 6 hrs

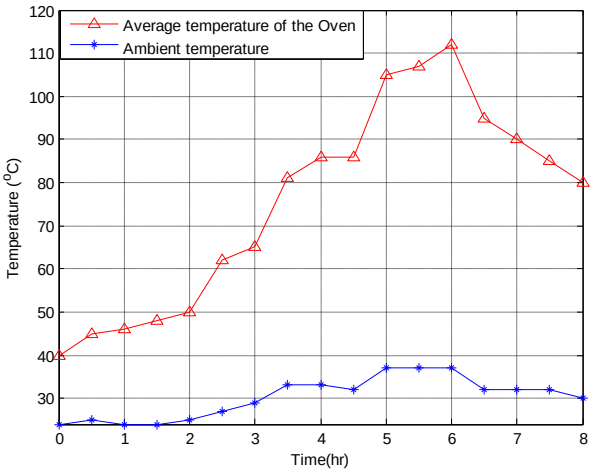

Figure 13. Experimental results of the solar oven

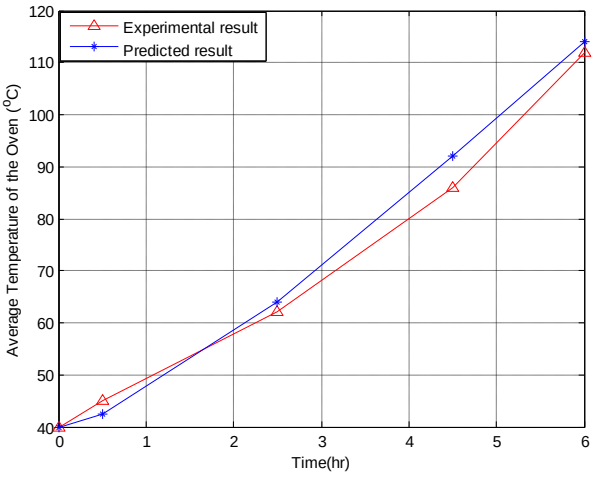

Figure 14. Comparison of Experimental results with model results

 ©2014 International Energy & Environment Foundation. All rights reserved.

5. Conclusion

In this work, mathematical models were developed and solved by using Characteristics-Based Split (CBS) Finite Element Method to numerically investigate the temperature, velocity and pressure distributions in solar oven. The numerical results were compared with the Experimental results and a good agreement ware found between the two results. The work will greatly assist in developing and optimising the design solar oven especially for the developing countries.

Nomenclature

Pr	Prandtl number	X	dimensionless length of the oven
Re	Reynold Number	y	breadth of the oven
Pe	Peclet number	Y	dimensionless breadth of the oven
t	time s	*Symbol*	
T	temperature, ^oC	α	thermal diffusivity, m^2/s
T_w	wall temperature, ^oC	θ	dimensionless temperature
T_∞	atmospheric temperature, ^oC	τ	dimensionless time
U	dimensionless velocity along x-axis	ρ	density, kg/m^3
u_∞	free stream velocity, m/s	μ	coefficient of dynamic viscosity, kg/ms
V	dimensionless velocity along x-axis	β	volumetric expansion coefficient
x	length of the oven, m		

References

[1] Adegoke, C. O. and Fasheun, T. A : Performance evaluation of a solar cooker under a tropical humid climate, Nigeria Journal of Renewable Energy, 1998, 6 (1-2) 71-74

[2] Amer, E. H: Theoretical and experimental assessment of a double exposure solar cooker, Energy Conversion and Management, 2003, 44, 2651-2663.

[3] Bello, A.M.A., Makinde, V., Sulu, H.T. Performance, tests and thermal efficiency of a constructed solar Box Cooker at a Guinea Savannah Station (Nigeria). J. American Science, 2010, 6, 32.

[4] Devadas, R. P An option for cooking solar energy, proceedings of the third international conference on solar cooker use and technology, Jan. 6-10, Coimbatore 641043 Tamil Nadu India, 1997, 15-17.

[5] Ekechukwu, O. V and Ugwuoke, N. T. Design and measured performance of a plane reflector augmented box type solar energy cooker, Renewable Energy, 2003, 28, 1935-1952.

[6] Franco, J., Cadena, C. and Saravia, L.: "Multiple use communal solar cookers". Solar Energy, 2004 77, pp. 217–223.

[7] Hussein, H. M. S, El-Ghetang, H. H and Nada, S. A. Experimental investigation of novel indirect solar cooker with indoor PCM thermal storage and cooking unit, Energy Conversion and Management , 2008, 49, 2237-2246.

[8] Kulkarni, S. S, Joshi, J. B., Pandit, A. B and Patel, S. B. Development of high efficiency concentrating solar cookers, Proceedings of the third International conference on solar cookers use and technology held between Jan 6-10 in Coimbatore, Tamil Nadu, India, 1997, 244-249

[9] Lof, G. O. G (1963): Recent investigations in the use of solar energy for cooking, Solar Energy, 1963, 7, 125.

[10] Malik, A. Q and Hamid Bin Hussen. Development of a solar cooker in Brunces Darussalam, Renewable Energy, 1996, 7 (4), 419-425.

[11] Negi, B. S and Purohit, I. Experimental investigation of a box type solar cooker employing a non-tracking concentrator, Energy Conversion and Management, 2005, 46, 577-605.

[12] Olusegun, H. D. Design construction and testing of a solar box cooker using locally sourced material, Journal of Research Information in civil engineering, 2006, 3, (1) 102-125.

[13] Patel, N. V. and Philip, S. K. Performance evaluation of three solar concentrating cookers, Renewable Energy, 2000, 20, 347-354.

[14] Babuska "The finite element method with Lagrangian multipliers" Number. Math., 1973, 20, 179-192.

[15] Brezzi F. "On the existence, uniqueness and approximation of saddle-point problems arising from Lagrangian multipliers." RAIRO Ser. Rouge, 1974, 8, 129-151.

[16] Lewis R.W., Nithiarasu P. and SeetharamuK.N. Fundamental of the Finite Element Method for Heat and Fluid Flow John Wiley and Sons, Ltd., 2004.

 ©2014 International Energy & Environment Foundation. All rights reserved.